Structure and elastic properties of amorphous silicon carbon nitride films

G. Lehmann and P. Hess*
Institute of Physical Chemistry, University of Heidelberg, D-69120 Heidelberg, Germany

J.-J. Wu, C. T. Wu, T. S. Wong, and K. H. Chen
Institute of Atomic and Molecular Sciences, Academia Sinica, Taipei, Taiwan

L. C. Chen
Center for Condensed Matter Sciences, National Taiwan University, Taipei, Taiwan

H.-Y. Lee
Research Division, Synchrotron Radiation Research Center, Hsinchu, Taiwan

M. Amkreutz and Th. Frauenheim
Department of Theoretical Physics, University of Paderborn, D-33098 Paderborn, Germany
(Received 22 March 2001; revised manuscript received 6 July 2001; published 3 October 2001)

Amorphous SiC_xN_y films with various compositions were deposited by ion-beam sputtering. The bonding characteristics, Young's modulus, and density of the films were investigated using x-ray photoelectron spectroscopy (XPS), Fourier-transform infrared (FTIR) spectroscopy, surface acoustic wave spectroscopy, x-ray reflection, and molecular-dynamics (MD) simulations. It was observed that the Young's modulus decreases from 260 ± 20 to 85 ± 12 GPa while the density decreases from 3.45 ± 0.2 to $2.3\pm0.3\,g/cm^3$ as the carbon content of the films increases from 0% to 68%. FTIR and XPS spectra indicate an increasing proportion of double and triple bonds with higher carbon content of the films. These experimental results were compared with the Young's moduli and the infrared spectra obtained from density-functional-based MD simulations. Also for these model calculations the Young's modulus drops from 237 ± 54 to 109 ± 25 GPa as the carbon content increases from 0% to 69%. It can be seen that the formation of C═C, C═N, C≡C, and C≡N bonds, together with the occurrence of terminating nitrogen atoms for the films with higher carbon content, are responsible for the degradation of the sp^3 network, and therefore for a lower Young's modulus and density.

DOI: 10.1103/PhysRevB.64.165305 PACS number(s): 68.60.Bs, 81.70.Cv, 31.15.Qg, 81.05.Gc

I. INTRODUCTION

The development of new materials or the modification of already known composites is a wide and important field of research in materials science and technology. For some purposes materials with versatile properties are needed, while other applications demand only a very specific behavior. Today, with the help of computer simulations, it is possible to estimate the physical and chemical properties of materials. As a result, great efforts are being made to synthesize materials for which excellent properties can be predicted.

One example is the covalently bonded β-C_3N_4. Based on an empirical approach, which takes into account the number of constituent elements (P), the interatomic distance (D), and the degree of bond covalence (C), a bulk modulus (B) can be predicted with the PDC model.[1]

$$B=12\,650P^{-0.0806}D^{-3.41}C^{0.318}.$$

For β-C_3N_4 the PDC model predicts a bulk modulus of 422 GPa and a hardness of 73 GPa. For diamondlike semiconductors made of group III-IV-V elements, estimates using this PDC model deviate on the average 1.8% from the measured values. With first-principles calculations, similar results have been obtained for this hypothetical material,[2] which are comparable with the bulk modulus of a diamond of 442 GPa.[3] However, although great efforts have been made, the growth of β-C_3N_4 crystallites large enough for analysis has not been reported yet. Nevertheless, for CN_x films with a structure of buckled graphite basal planes, in which the sp^2-bonded basal planes are terminated with N bonded to sp^3-hybridized carbon atoms, a hardness of 40–60 GPa could be demonstrated.[4] In contrast, the measured hardness of most reported CN_x films was in the range of 10–20 GPa, resulting from the presence of soft phases containing C═N and C≡N groups.

Besides carbon nitrides the synthesis of materials containing silicon in addition to carbon and nitrogen has grown in interest in recent years. To date several techniques have been developed to produce various kinds of Si-C-N composite (SiC_xN_y) films, which have excellent properties such as high oxidation resistance, wide band gaps, and promising mechanical properties.[5–12] Amorphous SiC_xN_y (a-SiC_xN_y) films synthesized by thermal chemical vapor deposition (CVD) techniques showed a hardness in the range of 27–38 GPa,[6] while a-SiC_xN_y films deposited by electron cyclotron resonance plasma CVD possessed a hardness of 22 GPa.[8] For crystalline Si-C-N films produced by microwave plasma CVD a hardness of 30 GPa and a bulk modulus of 322 GPa were reported.[8] Compared to the hardness predicted for the hypothetical β-C_3N_4, the values measured for the Si-C-N materials were much lower, although the addition of silicon

 ©2001 The American Physical Society

was expected to promote the formation of sp^3-hybridized carbons and also of additional bonds with nitrogen.[8]

In this study the proportions of Si, C, and N in the a-SiC_xN_y films deposited on silicon or fused silica substrates by ion-beam sputtering (IBS) were varied systematically to investigate the elastic and mechanical properties as a function of the carbon content. In parallel, computer simulations were performed to study the structural and elastic properties of the a-SiC_xN_y films. Different models of the amorphous network were generated with varying carbon content and microscopic mass densities corresponding to the IBS-deposited films.

The composition of the experimentally deposited films was determined by x-ray photoelectron spectroscopy (XPS). Fourier-transform infrared (FTIR) spectroscopy was applied to reveal the bonding configurations. Furthermore, surface acoustic wave spectroscopy (SAWS) was used to determine the Young's modulus and the density of the films. These experimental results were then compared with the Young's moduli and the infrared (IR) spectra calculated by the molecular-dynamics (MD) simulations. Additionally, the network characteristics of the simulated structures were analyzed. This information is expected to improve the understanding of the dependence of the mechanical properties on the carbon content at the molecular level.

II. EXPERIMENT

A. Deposition and film thickness

The IBS reactor employed to deposit the a-SiC_xN_y films has been described in more detail elsewhere.[13,14] A 3-cm Kaufman-type nitrogen ion source was used to sputter the target at a 45° angle of incidence. The distance between substrate and target was 20 cm. The target was a two-inch-diameter graphite sheet covered with a $(15\text{-mm})^2$ silicon wafer at the center, which was further covered with a typically $(10\text{-mm})^2$ SiC film. The size of the silicon wafer and the SiC film could be varied. By adjusting the sputter target and the N_2^+ beam voltage, films of various compositions were deposited on the Si(100) and fused silica substrates. The target holder was rotated at 40 rpm to ensure homogeneous sputtering. The base pressure of the deposition chamber was 0.1 mPa while the pressure during deposition was kept at 40 mPa. Apart from the heating caused by the ion-beam bombardment during deposition, no external heating of the substrate or target was employed. Thus, the deposition temperature was below 100 °C as measured by a thermocouple from the backside of the substrate.

The thickness of the a-SiC_xN_y films was determined by fitting the ellipsometric data obtained by variable angle spectroscopic ellipsometry (VASE), as well as by direct cross-section investigations using scanning electron microscopy. The films showed a thickness variation of less than 10% in the area investigated by SAWS. The surface roughness for a typical film thickness of 500 nm was in a range of 10 nm.

B. Composition and structure analysis

A Perkin Elmer Phi 1600 ESCA system with a $(800\text{-}\mu\text{m})^2$ sampling area and 11.75-eV pass energy was employed to analyze the compositions and the chemical bonding states of the films. MgK_α radiation of 1253.6 eV was used as an x-ray source. To obtain information about the chemical bonding states, scans of Si($2p$), C($1s$), and N($1s$) peaks of some of the a-SiC_xN_y films were performed. This has to be done on the as-deposited surfaces to avoid the destruction of the chemical bonding by Ar^+ bombardment. The spectral resolution was 0.7 eV. The composition of the films was obtained by depth profiling using XPS with Ar^+ bombardment of the samples.[15]

IR spectra were obtained in reflection mode with a Bomem MB series FTIR spectrometer under ambient conditions. The aim was to determine the chemical bonding configuration in the a-SiC_xN_y films and to correlate this information with the results on the dependence of the Young's modulus and density on the carbon content.

C. Elastic properties and density

To excite the surface acoustic wave (SAW) pulses a frequency-tripled Nd:yttrium aluminum garnet laser (wavelength $\lambda = 355$ nm) with a pulse duration of 8-ns full width at half maximum was focused to a line 10-mm long and 7-μm wide on the sample surface. Laser-pulse energies of 150–500 μJ were used. The SAW's were monitored with a piezoelectric polyvinylidenefluoride foil detector pressed onto the surface with a metal wedge.[16] The signal was amplified by a 60-dB high-frequency (1–500 MHz) amplifier (AU-4A-0150), recorded by a 500-MHz digital oscilloscope (Tektronik TDS 540), and averaged over 250 pulses to improve the signal-to-noise ratio. From Fourier transformation of a SAW pulse detected at two different propagation distances from the excitation source, the dispersion of the phase velocity was calculated.[17] To obtain the Young's modulus and the density of the films, theoretical dispersion curves were fitted to the experimental ones based on the theory for the propagation of linear SAW pulses in layered media.[18] As discussed in previous publications,[17,19–21] the dispersion curves depend on four film properties, namely, the Young's modulus, Poisson ratio, density, and thickness, as well as the elastic constants and density of the substrate, which, however, are well known for the fused silica and single-crystal silicon.

In order to confirm the densities derived from the SAW measurements, three a-SiC_xN_y films were examined independently using the x-ray reflectivity (XRR) technique.[22] The XRR measurements were carried out at the in-house x-ray laboratory of the Synchrotron Radiation Research Center in Hsinchu, Taiwan, using a Mac Science M1 8XHF rotating anode x-ray generator. A copper target was used to provide the characteristic x-ray radiation of 8.05 keV. The incident beam was monochromatized by a flat Ge(111) crystal. The undesirable Cu$K_{\alpha 2}$ radiation was eliminated by two sets of slits. By applying another two pairs of slits between sample and detector, the typical wave-vector resolution in the scattering plane was set to approximately 0.0015 Å^{-1} in these experiments. The density of the films was determined by the critical angle (θ_c) of the x-ray reflectivity curve, at which the reflectivity of the sample has its maximum. The final value of θ_c is converted to the mass density of the films

by using the formula for low atomic number material $\theta_c = 1.64\times 10^{-3}\cdot\lambda\cdot\rho^{1/2}$,[22] where λ is the wavelength of the x-rays in angstroms and ρ is the mass density of the material [g/cm^3].

III. STRUCTURE SIMULATION

A. Molecular-dynamics simulation

All the models of the amorphous network are created by density-functional molecular-dynamics (MD) simulations, in which the interatomic forces are calculated on a quantum-mechanical basis. The method used is based on a density-functional nonorthogonal tight-binding (DFTB) scheme,[23–25] wherein the Kohn-Sham orbitals of the atomic configuration are related to a minimal basis of atom-centered valence electron orbitals of all atoms. The effective one-electron potential of the many-atom structure in the Kohn-Sham equation is approximated by a sum of contracted pseudoatom potentials.[26] The related valence electron orbitals in a Slater-type representation and the contracted pseudoatom potentials are determined from self-consistent single-atom density-functional calculations within the local-density approximation (LDA).[23]

According to this approximation only two-center Hamiltonian matrix elements are taken into account, leading to a simplified eigenvalue problem for the single-particle electron energies. The two-center Hamiltonian matrix elements and the overlap matrix elements are calculated from the set of determined basis functions and pseudoatom potentials.

The total energy then consists of the sum over all occupied cluster electron energies, the so-called band-structure energy, and a repulsive pair energy that includes the double-counting exchange and correlation contributions as well as the core-core repulsion. This repulsive energy is determined as a superposition of short-range repulsive pair interactions as a function of distance by taking the difference of the self-consistent field LDA cohesive energy and the corresponding DFTB electronic energy for a suitable reference system. This method has been generalized and optimized for molecular-dynamics investigations of structure formation within three-dimensional periodic supercells[27,28] and has already been applied successfully to study the structure and properties of other amorphous materials.[29–33]

B. Simulation of deposition

To model the a-SiC$_x$N$_y$ films, MD simulations for 224 atoms (for the models K_{MD} and L_{MD} corresponding to the experimentally deposited samples K_{exp} and L_{exp}) and 240 atoms (models A_{MD}, H_{MD}, and I_{MD} with varying compositions of silicon, carbon, and nitrogen have been made. The atoms were enclosed within a simple cubic periodic supercell with fixed volume according to the given microscopic mass density of the corresponding experimental film. Thus, the microscopic mass density serves as input parameter for the MD simulations together with the composition of the film.

To simulate the experimental situation the initial structures did not have a randomized configuration of silicon and carbon but were arranged correspondingly to the arrangement of the laminated targets described before. In addition, nitrogen atoms were inserted randomly to simulate the N_2^+ beam.

As the relaxation regime for the structure formation, the model systems were first heated for 1 ps from 300 to 4000 K with a linear increase in temperature. After that the structure was equilibrated at a constant temperature of 4000 K for 1 ps followed by a 1-ps cooling to 300 K and again equilibrated for another 1 ps at 300 K. Then, a relaxation with a conjugate gradient algorithm was applied for structural optimization and energy minimization. The high temperature in the simulation was needed to enforce amorphization and compensate the short-time intervals due to computational limits.

Only for sample L_{MD}, with the highest carbon content, was this procedure not sufficient. Sample L_{MD} still had a small amount of terminating carbon atoms with dangling bonds after relaxation. This is thought to be due to the small density of this model so that a longer annealing process would presumably lead to a better network connectivity.[30,31] Nevertheless, this model is included, since it shows the right tendency in describing the properties of the corresponding experimental sample.

Other relaxation regimes have been tested, for example, starting with 8000 K, which is the standard method usually applied for amorphous models. However, this did not yield promising structures since any memory of the starting configuration is lost.

C. IR spectra and Young's modulus

In addition to the experimental IR spectra, the theoretical IR spectra of the post-relaxed structures generated by MD simulations were calculated. From these computations, spectra consisting of single delta peaks were obtained. A Gaussian broadening was applied to the single delta peaks to adapt to the experimental conditions so that the IR spectra could be compared with the measured ones. This provided additional chemical bonding information about the structure and the dependence of the properties on the carbon content. Furthermore, by comparing the calculated and measured spectra, the agreement between simulated and real structures of the composites could be estimated.

To obtain the Young's modulus E for the MD-simulated samples, first the bulk modulus B of the structures was calculated from their total-energy curves by determining the curvature and using $B = V_0 d^2E_{\mathrm{tot}}(V)/dV^2|_{V=V_0}$. This was followed by the calculation of the Young's modulus for isotropic materials according to $B = E/[3(1-2\nu)]$ with a given Poisson ratio ν.[34]

IV. RESULTS

A. Bonding and structure

1. Fourier-transform infrared spectroscopy

Characteristic IR spectra of the a-SiC$_x$N$_y$ films with various values of x and y are depicted in Fig. 1, specifically, samples A_{exp}, C_{exp}, H_{exp}, K_{exp}, and L_{exp}. In order to emphasize the change of the IR spectra with increasing carbon

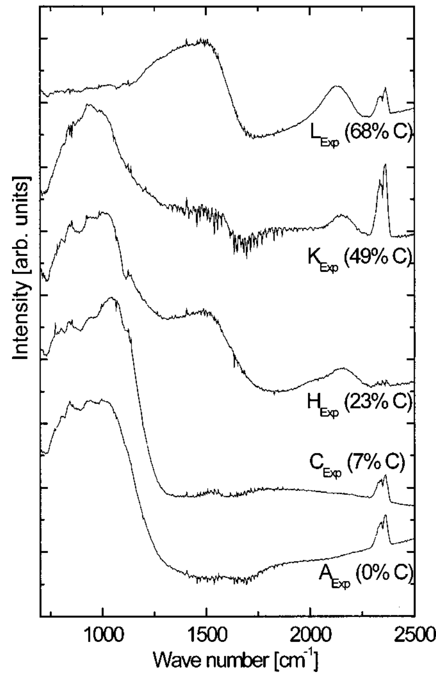

FIG. 1. IR spectra of the a-SiC_xN_y films with various compositions. To show all curves in one single graph the intensity is shifted for the different samples and no absolute values are given.

content these spectra are shown in a single graph with an arbitrary offset. In Fig. 2 the experimental and the Gaussian-broadened spectra of the MD simulations of the samples A [Fig. 2(a)], *H* [Fig. 2(b)], and *L* [Fig. 2(c)] are compared. In addition, the delta peak spectra initially obtained by the simulations are presented.

Regarding the experimental data, it can be seen that all samples show a broad peak at a wave number around 950 cm^{-1}, except for sample L_{exp} with the lowest Si and the highest C contents (Fig. 1). This wave-number range is assigned mainly to Si-N bonds.[35] With increasing carbon content, a second peak at approximately 1500 cm^{-1} rises while an additional peak at 2150 cm^{-1} occurs for films with more than 20% carbon.

To analyze these changes in the experimental IR spectra in more detail, a comparison with the spectra obtained from MD simulations is helpful (Fig. 2). The IR spectrum of A_{MD} clearly indicates a first peak at 550 and a second at 950 cm^{-1} [Fig. 2(a)]. Due to the mercury-cadmium-telluride (MCT) detector's cutoff frequency, no reliable data is available below a wave number of 700 cm^{-1} for the experimental spectra. The second peak from sample A_{MD} agrees very well with the experimental spectrum. The main contribution to both peaks originates from various types of Si-N-Si bending modes. The shoulder in the spectrum of A_{MD} of the Si-N peak at 1250 cm^{-1} is less pronounced in the experimental spectrum.

A closer look at the delta peaks of H_{MD} [Fig. 2(b)] reveals that the peak at 1470 cm^{-1} belongs to sp^2-hybridized carbon (C═C and C═N) and C-N ring structures, while another peak at 2150 cm^{-1} corresponds to sp^1-hybridized carbon (C≡N). This is in good agreement with other findings.[36] For the wave-number range 500–1000 cm^{-1} a lot of small con-

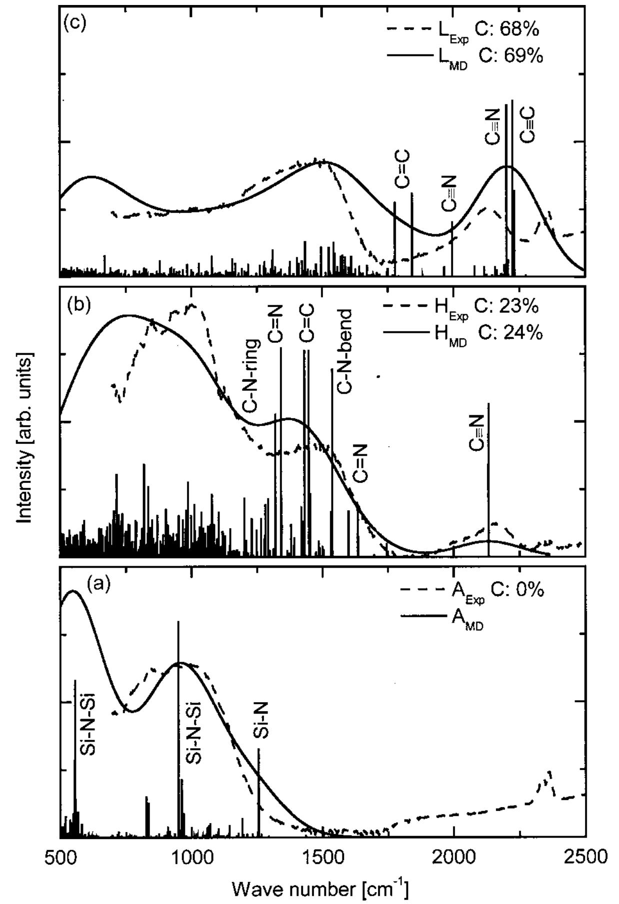

FIG. 2. Comparison between the IR spectra obtained experimentally (dashed line) and by MD simulation (solid line) for samples *A*, *H*, and *L*. The simulated IR spectra consist of an overlap of different single delta peaks (also shown in the graph) that are Gaussian broadened to simulate the experimental conditions.

tributions result in a broad peak for the MD-simulation spectrum. Except at wave numbers below 800 cm^{-1}, where the sensitivity of the MCT detector is low, the experimental and theoretical spectra agree very well for sample *H*.

Additional contributions from sp^1-hybridized carbon (C≡C and further C≡N) lead to a substantial increase of the peak at 2150 cm^{-1} for the sample *L* [Fig. 2(c)]. The other main peak for sample *L*, around 1500 cm^{-1}, is related to a growing proportion of sp^2-hybridized carbon in the film. The contribution of the Si-N bonds at 950 cm^{-1} is much smaller for this sample than for the samples with lower carbon content, indicating a decrease of these bonds due to the decreasing silicon content. Some minor deviations can be found between the MD and experimental spectra, for example, the shoulder at approximately 1750 cm^{-1} of L_{MD} is quite pronounced, whereas in the spectrum of L_{exp} it seems to be less than half this size. In conclusion, apart from the missing experimental data below 700 cm^{-1}, a reasonable agreement concerning peak positions and relative peak heights between the experimental and simulated IR spectra was obtained.

The relatively sharp double peak at 2350 cm^{-1}, which is present in the experimental IR spectra but not in the MD

TABLE I. Composition and elastic properties of a-SiC_xN_y films deposited by ion-beam sputtering and calculated by MD simulation.

	Composition (percent)[a]				Thickness (μm)	Young's modulus (GPa)	Density[b] (g/cm^3)
Sample	C	N	Si	O			
A_{exp}	0	49	44	7	7.79±0.05	260±20	3.45±0.2
A_{MD}	0	53	47			237±54	3.4
B_{exp}	5	36	51	8	0.25±0.03	230±30	3.15±0.25
C_{exp}	7	43	43	7	1.35±0.25	235±30	3.2±0.2
D_{exp}	9	39	44	8	0.31±0.03	235±20	3.2±0.2 (3.2±0.15)
E_{exp}	12	36	46	6	1.62±0.1	245±20	3.25±0.15
F_{exp}	12	38	45	5	0.31±0.03	245±25	3.35±0.25
G_{exp}	22	40	34	4	0.53±0.05	225±15	3.3±0.2
H_{exp}	23	32	40	5	0.61±0.06	220±20	3.15±0.25
H_{MD}	24	34	42			223±51	3.2
I_{exp}	32	32	32	4	0.6±0.06	200±20	3.2±0.35
I_{MD}	33	33	33			178±40	3.1
J_{exp}	36	24	29	11	0.3±0.03	190±30	2.65±0.4 (2.84±0.14)
K_{exp}	49	21	20	10	0.25±0.03	130±20	2.5±0.45
K_{MD}	55	23	22			143±33	2.75 (2.75±0.14)
L_{exp}	68	22	9	1	0.54±0.01	85±15	2.3±0.3
L_{MD}	69	22	9			109±25	2.35

[a]Composition was determined by XPS. For the MD-simulation samples, these values were set as initial conditions.

[b]Density measured by the x-ray reflectivity method is shown in parentheses.

simulations, is due to CO_2 absorption in the ambient air, and therefore not a characteristic of the film.

2. XPS and MD-simulations bonding analysis

The results of the film composition obtained by XPS depth profiling[15] are shown in Table I, together with the results of SAWS. The XPS depth profile measurements showed less than 5% fluctuation of the composition except near the surface of the films, where higher carbon and oxygen contents were observed due to surface contamination. With the XPS scans of the C(1s), N(1s), and Si(2p) peaks, information about the bonding behavior could be obtained and compared with the MD simulations.

For the components present in our films, the XPS spectrum belonging to the C(1s) consists of five components, centered at 282.8 (C-Si), 284.6 {C bonded to sp^2-hybridized C[C(sp^2)-C]}, 285.8[C(sp^2)-N], 287.0[C(sp^3)-N], and 288.9 eV (C-O).[37] The contributions at 397.8 and 399.3 eV in the N(1s) peak are related to N-Si and N-C(sp^2), respectively. In the Si(2p) spectrum, although the Si-Si (99.2), Si-C (100.3), Si-N (102.0), Si-O_2(103.3), and Si-O (104.5 eV) single bonds contribute to this spectrum, the Si(2p)-N peak is by far the strongest.

Figure 3 shows the XPS spectra of sample G_{exp}, with a composition of 22% C, 40% N, 34% Si, and 4% O. The area ratio of the Si-Si to the Si-N peak was less than 1/10, suggesting that the major part of Si within the film was bonded

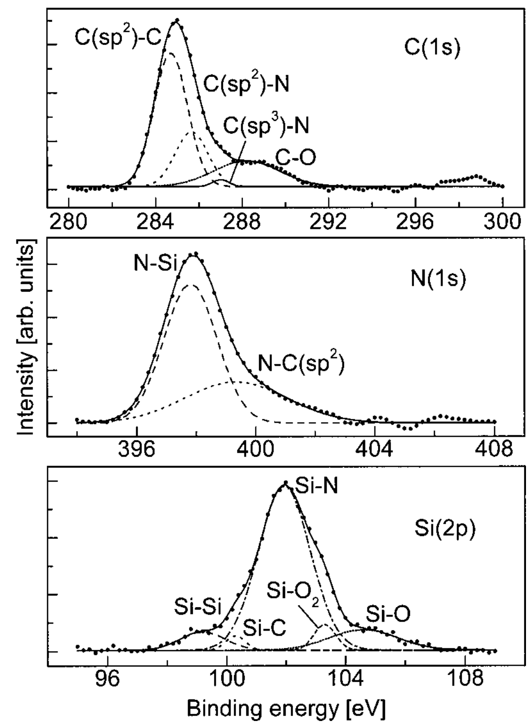

FIG. 3. XPS spectra of C(1s), N(1s), and Si(2p) for the a-SiC_xN_y film G_{exp} with a composition of 22% C, 40% N, 34% Si, and 4% O.

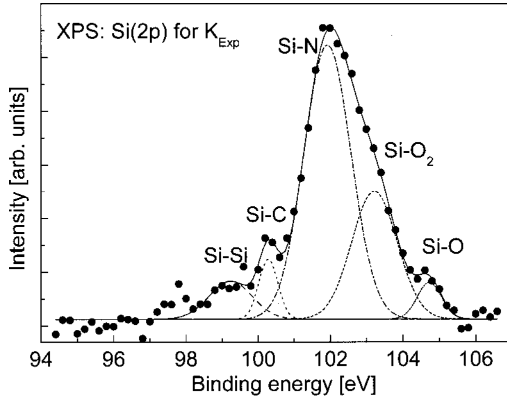

FIG. 4. XPS spectrum of Si$(2p)$ for the a-SiC_xN_y film K_{exp} with a carbon content of 49%.

to N. Notably, there was no major peak that matches the Si-C bonding energy at 100.3 eV in the Si$(2p)$ spectrum and no peak at 282.8 eV in the C$(1s)$ spectrum, suggesting that Si-C bonds were almost missing in this film. Also, only a minor peak at 287.0 eV, attributed to sp^3-hybridized C bonded to N[C(sp^3)-N], could be found. Even in the sample K_{exp} with a carbon content of 49% (21% Si, 20% N, and 10% O as impurity), the Si-C phase detected was in the range of only 5% (Fig. 4). The C-O peaks in the C$(1s)$ scans as well as the Si-O peaks in the Si$(2p)$ scans became smaller after sputtering with Ar^+, indicating that the major part of these bonds resulted from contamination on the surface due to air exposure.

In general it can be concluded from the spectra that the major part of the bonding is between Si and N and between C and C or N. The small proportion of Si-C bonds in the films is quite surprising, especially for films with a high carbon content. Moreover, this is in contradiction with the MD simulations. In Table II and Fig. 5, the binding properties obtained from a geometrical analysis of the structure of the MD-simulation models are shown. Looking at the XPS data of G_{exp} (given in Fig. 3), the composition of which is comparable to that of H_{MD} (see Table I), it can be seen from Table II that the ratio of Si-N bonds to N bonded with sp^2-hybridized C[N-C(sp^2)] and Si-N to Si-Si bonds of

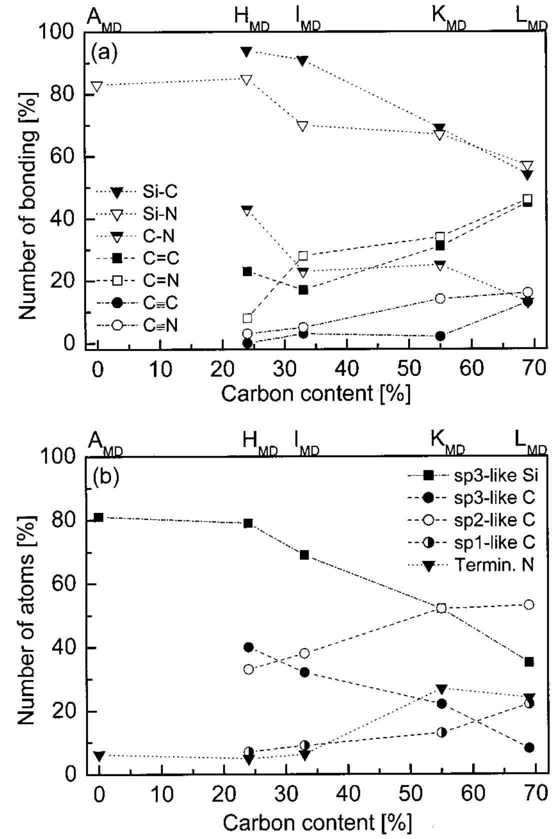

FIG. 5. (a) Number of double and triple bonds (C=C, C=N, C≡N, and C≡C) and number of single bonds (Si-C, Si-N, and C-N) related to the total number of bonds of this kind (e.g., the number of C=N double bonds related to all C bonded with N) obtained from the geometrical analysis of the MD models. (b) Carbon and silicon hybrid fractions and percentage of terminating nitrogen atoms obtained from the geometrical analysis of the MD models.

H_{MD} is very similar to those obtained for G_{exp} from the XPS experiment. However, in contrast to the experimental XPS data there are many more Si-C bonds in the model structure. This is confirmed by the coordination number of Si-C (the

TABLE II. Binding properties of a-SiC_xN_y films obtained by MD simulation. The total number of the specified kind of bond and the total number of all bonds in the periodic supercell related to the carbon content of the films are given.

	A_{MD}	H_{MD}	I_{MD}	K_{MD}	L_{MD}
C content (percent)	0	24	33	55	69
Si-C		112	103	84	41
Si-N	328	182	125	42	14
Si-Si	56	42	33	21	4
C(sp^3)-N		16	19	18	12
C(sp^2)-N		18	48	45	65
C(sp^2)-C		16	23	71	101
Total number of all bonds in periodic supercell	384	395	378	326	290

TABLE III. Coordination numbers of a-SiC_xN_y films obtained by MD simulation.

		A_{MD}	H_{MD}	I_{MD}	K_{MD}	L_{MD}
Coordination number	SiC		1.12	1.29	1.68	2.05
	SiN	2.88	1.82	1.56	0.84	0.70
	SiSi	0.98	0.84	0.82	0.84	0.40
	Si	3.86	3.78	3.67	3.36	3.15
	CC		0.76	0.88	1.64	1.69
	CN		0.64	1.02	0.65	0.66
	CSi		1.93	1.29	0.69	0.27
	C		3.33	3.19	2.98	2.62
	NC		0.45	1.02	1.52	2.02
	NSi	2.60	2.22	1.56	0.81	0.28
	N	2.60	2.67	2.58	2.33	2.30

mean number of bonds between silicon and carbon) and the total coordination number of Si (see Table III). Moreover, sp^3-hybridized C bonded to N is observed.

For K_{exp} and K_{MD} the same difference between XPS measurement and MD simulation is found: the number of Si-C bonds for K_{MD} is even larger than that of Si-N bonds (Table II) and again C(sp^3)-N appears. But for K_{exp} the area under the Gaussian fit curve of the Si-C bonds is only 1/10 of the curve of the Si-N bonds (Fig. 4).

In addition, the coordination numbers of Si-C and N-C are larger for K_{MD} than for H_{MD}, a fact which may be attributed to the increased carbon content. This is compatible with the decreased coordination numbers of N-Si and Si-N.

From the MD simulation [see Fig. 5(a)] it is obvious that with increasing carbon content the proportion of single bonds (Si-N, C-N, and Si-C) decreases, while the proportion of double and triple bonds (C═N, C═C, C≡N, and C≡C) increases. Only I_{MD} does not fit exactly into this behavior having too small a number of C-N bonds and C═C bonds, as can be seen in Fig. 5(a). This is due to the existence of many N═C═N bonds, which were already present in the MD initial structure of I_{MD} (and only for I_{MD}) resulting from the random insertion of nitrogen.

This is in good agreement with the decreasing proportion of sp^3-like Si and C and the increasing contribution of sp^2-like and sp^1-like C atoms with increasing carbon content, as can be seen from Fig. 5(b). In addition, the number of terminating nitrogen atoms stays nearly constant at 5%–6% up to a carbon content of 33% and then increases at once to almost 26% for films with higher C content. It should be noted here that for all components a mixed type hybridization is allowed, a so-called $sp^{(2+x)}$ hybridization, which also decreases with increasing carbon content for all components.

Regarding the total coordination numbers calculated by the MD simulations (Table III) it can be seen that the coordination number for nitrogen stays nearly constant at 2.3–2.6, indicating that the silicon atoms are replaced one by one by carbon. For carbon it decreases from 3.3 to 2.6, inducing a weakening of the stiffness of the structure. The coordination number for silicon changes from approximately four neighbors to about three with increasing carbon content. Hence, the coordination number for silicon differs from its usual value of four, but this has already been observed before, e.g., for a-Si:H films,[38,39] where dangling bonds are responsible for a lower coordination number.

B. Young's modulus and density

The SAW experiments yielded an anomalous dispersion for all films deposited on fused silica. This behavior is connected with the fact that the SAW's propagate faster in the film than in the substrate. Similarly, SAW's in the samples A_{exp}, G_{exp}, H_{exp}, and I_{exp} propagating in the ⟨100⟩ direction of the Si(100) substrate plane showed anomalous dispersion and only for sample L_{exp} was normal dispersion found. For SAW propagation in the ⟨110⟩ direction, the samples G_{exp}, I_{exp}, and L_{exp} exhibited normal dispersion, whereas for sample A_{exp} the velocity first increased with increasing frequency, but at a frequency higher than 100 MHz the velocity decreased. Usually the dispersion curves could be fitted in the frequency range of 20–150 MHz or even higher.

The shape of the dispersion curves was not characteristic enough to obtain the full set of the four elastic and mechanical film properties; only two of them could be determined. Therefore, the thickness had to be measured independently. In addition, the Poisson ratio, which is not a critical film property with respect to curve fitting, was chosen to be $\nu = 0.28 \pm 0.05$, according to previous studies on the mechanical properties of SiN films.[40] However, the uncertainty in the Poisson ratio and some variation (up to 10%) in the thickness of the films are the main contributors to the error of up to 15% given for the Young's modulus and the density.

The measured anomalous dispersion curve and the corresponding theoretical fit for the sample C_{exp} are illustrated in Fig. 6(a). The velocity at the low frequency corresponds to the Rayleigh velocity of the pure fused silica substrate and increases with higher frequencies. For the films deposited on Si(100) the measurements were carried out in the ⟨100⟩ and ⟨110⟩ directions and produced two independent sets of consistent data. The measured dispersion curves and the corresponding theoretical fits for the A_{exp} film on a Si(100) sub-

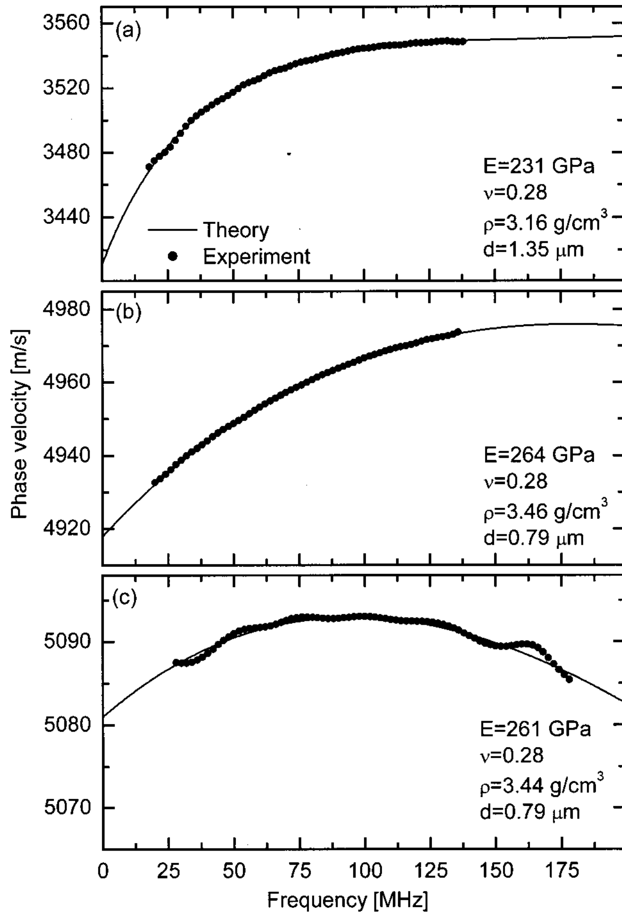

FIG. 6. (a) Dispersion curve of the a-SiC_xN_y film C_{exp} on the fused silica substrate. (b) and (c) Dispersion curves of the SiN film A_{exp} on Si(100) measured in the ⟨100⟩ and ⟨110⟩ directions, respectively.

strate are presented in Figs. 6(b) and 6(c) for the ⟨100⟩ and ⟨110⟩ directions, respectively. All results obtained by the SAW measurements are listed in Table I, together with the composition results of the XPS analysis and the VASE thickness values.

Figure 7 presents the correlation between the Young's modulus [Fig. 7(a)] and density [Fig. 7(b)] of the a-SiC_xN_y films and the carbon content determined by XPS measurements. As illustrated in Fig. 7(a), the Young's modulus of the films with a carbon content below 12% remains essentially constant at about 240 GPa, within the error bars, which is comparable to that of the SiN film. However, as the carbon content increases further, the Young's modulus decreases significantly. At a carbon content of 68%, the Young's modulus is reduced to only 85 ± 15 GPa. A similar trend is observed for the density of the a-SiC_xN_y films. As shown in Fig. 7(b), the density is nearly constant at about 3.2 g/cm^3 for films with a carbon content below 23% and then drops to 2.3 g/cm^3 for the highest carbon content investigated.

With XRR a critical angle of 0.217° was measured for the fused silica substrate. The resulting density is 2.23 ± 0.13 g/cm^3, which is in good agreement with the value of

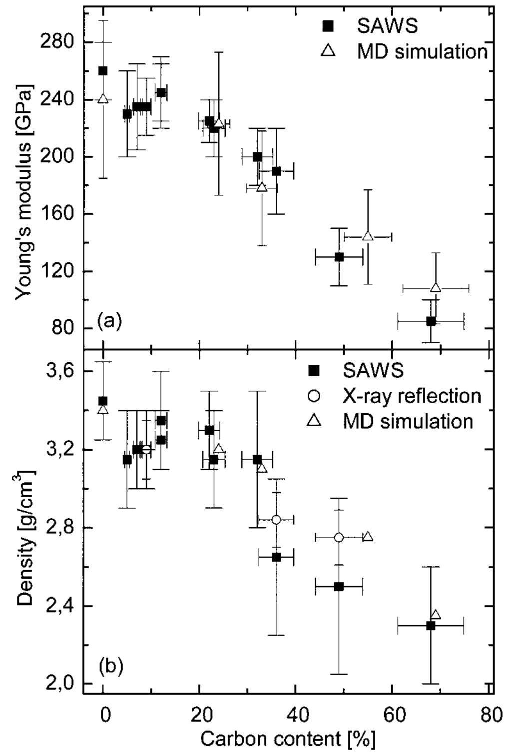

FIG. 7. Dependence of the Young's modulus (a) and the density (b) of the a-SiC_xN_y films on the carbon content. The SAWS results are plotted as filled squares, the MD simulations as triangles, and the XRR as circles.

2.203 g/cm^3 provided by the producer of the substrate (Heraeus). The critical angles of the samples D_{exp}, J_{exp}, and K_{exp} were 0.26°, 0.245°, and 0.241° (see Fig. 8) and the corresponding densities were 3.2 ± 0.15, 2.84 ± 0.14, and 2.75 ± 0.14 g/cm^3, respectively. These values agree well with the results of the SAW experiments (see Table I).

For the evaluation of the Young's modulus from the MD-simulation models, a Poisson ratio of $\nu=0.28\pm0.05$ was assumed, as was done for the evaluation of the SAW experiments. From this we obtained the Young's moduli listed in Table I by using $E=3(1-2\nu)B$ for isotropic materials,[34] as mentioned before.

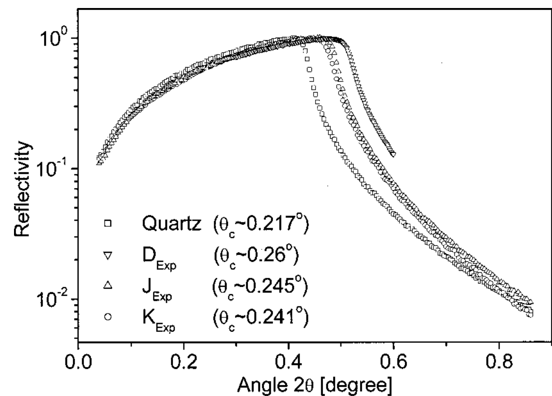

FIG. 8. The XRR curves and critical angles of the fused silica reference and the a-SiC_xN_y films D_{exp}, J_{exp}, and K_{exp}.

It can be seen that the calculated values differ slightly from the measured ones but they all show the same tendency related to the carbon content as those determined by the SAW measurements: there is a decrease in the Young's modulus from 237 to 109 GPa as the carbon content increases from 0% to 69% and the mass density decreases in good agreement with the experimentally observed behavior [Fig. 7(b)]. The high error for A_{MD}, H_{MD}, and I_{MD} is due to the relatively large deviation of ± 0.05 chosen for the Poisson ratio in the SAW experiments.

V. DISCUSSION

The properties of the IBS-deposited a-SiC_xN_y films as well as of the MD-simulated models of the films depend greatly on the composition of the films, especially on the carbon content. The SAW measurements show that the Young's moduli and the densities of the a-SiC_xN_y films with lower carbon content are nearly constant. The Young's modulus has a value of about 240 GPa for films with a carbon content up to 12%. The range of the carbon content in which the film density stays around 3.2 g/cm^3 even goes up to 23%. The highest Young's modulus and density were reached by the pure SiN sample, with 260 ± 20 GPa and 3.45 ± 0.2 g/cm^3, respectively. The Young's modulus reported in the literature varies between 150 and 373 GPa for plasma-enhanced CVD (PE CVD) SiN_x films,[41] depending on the N-fraction x and the measurement method: 222 ± 3 GPa for a low pressure CVD SiN film,[40] and 310 GPa for single-crystal Si_3N_4.[41] These values are in agreement with the Young's modulus of 237 ± 54 GPa obtained by MD simulations in this study. The density is slightly higher than the densities of 2.62–3.0 g/cm^3 given for the PE CVD SiN films[41] and is quite similar to the density of crystalline Si_3N_4, reported to be between 3.19 and 3.44 g/cm^3.[41,42]

At higher carbon content, the Young's modulus and the density decrease significantly. A similar behavior is found for carbon incorporation in cubic boron nitride films,[43] where the Young's modulus is nearly constant at about 300 GPa for films with a carbon content from 3% to 6.2% but then drops to 100 GPa for a carbon content of about 11.8%.

From the IR spectra it is seen that the increase of the sp^2-hybridized carbon (C═C and C═N bonds) are expected to contribute to this behavior. In fact, carbon double bonds may increase the stiffness in a plane (e.g., graphite) but not in a three-dimensional network. It turns out that the decrease of the Young's modulus and especially of the density are not very pronounced for the samples whose IR spectra show no absorption peak at 2150 cm^{-1}. This peak is attributed to carbon triple bonds (C≡C and C≡N) and appears only for samples with a carbon content higher than 23%. Since with the triple bonds "chains" can be formed but not a two- or even three-dimensional network, this leads to a softening of the material. In addition, terminating groups are easily formed by triple bonds in nitrogen. This may result in larger vacant spaces or voids and therefore in a low-density and low network connectivity and so explains the decrease of the Young's modulus.

The models for the a-SiC_xN_y films computed by MD simulations provide more data for an understanding of this behavior. The proportion of sp^2-hybridized C increases from 32.8% (H_{MD}) to 52.6% (L_{MD}) [see Fig. 5(b)] while the proportion of sp^1-hybridized C increases from 6.9% to 22.1% for these samples. In addition, for H_{MD} 4.9% of the N atoms and for sample L_{MD} 24% of the N atoms have only one neighbor. Furthermore, it can be seen from the decreasing coordination numbers for all components of the films (Table III) that the connectivity of the molecular network is weaker for films with higher carbon content.

Finally, we briefly discuss to what extent the experimental findings can be supported by the MD-simulation models. It is likely that the models applied do not represent exactly the structure of the films deposited by IBS because they show a significantly higher content of Si-C bonds than could be detected by XPS for the IBS-deposited films. While the lack of Si-C bonds has been reported previously for amorphous[44] and crystalline[10,45] SiC_xN_y films, a high content of these bonds was found experimentally for other a-SiC_xN_y films.[46] So, this is still a point of discussion. Also, small deviations in the IR spectra between the modeled systems and the measurements are present. In any case, the general behavior of the IR spectra, as well as the density and the elastic properties, are similar for both approaches. In addition, it can be assumed that a large part of these deviations also comes from the difference in the proportion of the Si-N and Si-C contents. Altogether, provided these deviations are borne in mind, it can be justified to compare the experiments with the simulations and to explain, at least qualitatively, the experimental findings by means of the properties of the simulated structures.

VI. CONCLUSION

The correlation of elastic properties with the carbon content of ion-beam-sputtered a-SiC_xN_y films has been studied using SAWS, XPS, and FTIR techniques. Furthermore, MD simulations have been performed to simulate selected model systems and their properties. It turns out that the increased incorporation of carbon reduces the Young's modulus and the density of the films. While the Young's modulus only slightly decreases for films with low carbon content, a significant reduction of the stiffness has been observed as the carbon content increases above 12%. This can be explained with the results of the FTIR and XPS spectra and the MD simulations, which indicate the appearance of C═C, C═N, C≡C, and C≡N bonds in the samples with higher carbon content. Thus, the observed variation in the elastic and mechanical properties can be attributed to an increasing fraction of these low-coordination bonds in the amorphous network that diminishes the three-dimensional connectivity and stiffness. These stronger bonds with higher bond order may also induce structural defects that reduce the density. In addition, the increasing proportion of terminating nitrogen atoms may cause small voids that further decrease the density.

ACKNOWLEDGMENTS

The authors G. L., P. H., J. J. W., C. T. W., and K. H. C. thank the DAAD and NCS for financial support of the Taiwan-Germany exchange program. Additional financial support for G. L. from DFG is gratefully acknowledged. L. C. C. also thanks the NSC and Ministry of Education in Taiwan for financial support. M. A. and T. F. gratefully acknowledge support from the DFG Schwerpunktprogramm ‘‘Precursorkeramik.’’

*Email address: Peter.Hess@urz.uni-heidelberg.de

[1] C. M. Sung, Mater. Chem. Phys. **43**, 1 (1996).
[2] A. Y. Liu and M. L. Cohen, Science **245**, 841 (1989).
[3] H. J. McSkimin and W. L. Bond, Phys. Rev. **105**, 116 (1957).
[4] H. Sjostrom, L. Hultman, J.-E. Sundgren, S. V. Hainsworth, T. F. Page, and G. S. A. M. Theunissen, J. Vac. Sci. Technol. A **13**, 1063 (1995).
[5] M. Moriyama, K. Kamata, and I. Tanabe, J. Mater. Sci. **26**, 1287 (1991).
[6] A. Bendeddouche, R. Berjoan, E. Beche, and R. Hillel, Surf. Coat. Technol. **111**, 184 (1999).
[7] L. C. Chen, C. K. Chen, S. L. Wei, D. M. Bhusari, K. H. Chen, Y. F. Chen, Y. C. Jong, and Y. S. Huang, Appl. Phys. Lett. **72**, 2463 (1998).
[8] L. C. Chen, K. H. Chen, S. L. Wei, P. D. Kichambare, J. J. Wu, T. R. Lu, and C. T. Kuo, Thin Solid Films **355-356**, 112 (1999).
[9] G. Sato, E. C. Samano, R. Machorro, and L. Cota, J. Vac. Sci. Technol. A **16**, 1311 (1998).
[10] F. J. Gomez, P. Prieto, E. Elizalde, and J. Piqueras, Appl. Phys. Lett. **69**, 773 (1996).
[11] R. Riedel, H. Kleebe, H. Schonfelder, and F. Aldinger, Nature (London) **374**, 13 (1995).
[12] Th. Frauenheim, G. Jungnickel, P. Sitch, M. Kaukonen, F. Weich, J. Widany, and D. Porezag, Diamond Relat. Mater. **7**, 348 (1998).
[13] J.-J. Wu, T.-R. Lu, C.-T. Wu, T.-Y. Wang, L.-C. Chen, K.-H. Chen, C.-T. Kuo, T.-M. Chen, Y.-C. Yu, C.-W. Wang, and E.-K. Lin, Diamond Relat. Mater. **8**, 605 (1999).
[14] J. J. Wu, C. T. Wu, Y.-C. Liao, T. R. Lu, L. C. Chen, K. H. Chen, L. G. Hwa, C. T. Kuo, and K. J. Ling, Thin Solid Films **355-356**, 417 (1999).
[15] S. Hofmann, *Practical Surface Analysis by Auger and X-Ray Photoelectron Spectroscopy*, edited by D. Briggs and M. P. Seach (Wiley, New York, 1983), p. 143.
[16] H. Coufal, R. Grygier, P. Hess, and A. Neubrand, J. Acoust. Soc. Am. **92**, 2980 (1992).
[17] A. Neubrand and P. Hess, J. Appl. Phys. **71**, 277 (1991).
[18] G. W. Farnell and E. L. Adler, *Physical Acoustics* edited by W. P. Mason and R. N. Thurston (Academic, New York, 1972), Vol. IX, p. 35.
[19] A. A. Kolomenskii, M. Szabadi, and P. Hess, Appl. Surf. Sci. **86**, 591 (1995).
[20] R. Kuschnereit, H. Fath, A. A. Kolomenskii, M. Szabadi, and P. Hess, Appl. Phys. A: Mater. Sci. Process. **A61**, 269 (1995).
[21] P. Hess, Appl. Surf. Sci. **106**, 429 (1996).
[22] C. A. Lucas, P. D. Hatton, S. Bates, W. Ryan, S. Miles, and B. K. Tanner, J. Appl. Phys. **63**, 1936 (1988).
[23] D. Porezag, Th. Frauenheim, T. Köhler, G. Seifert, and R. Kaschner, Phys. Rev. B **51**, 12 947 (1995).
[24] Th. Frauenheim, F. Weich, T. Köhler, S. Uhlmann, D. Porezag, and G. Seifert, Phys. Rev. B **52**, 11 492 (1995).
[25] J. Widany, Th. Frauenheim, D. Porezag, T. Köhler, and G. Seifert, Phys. Rev. B **53**, 4443 (1996).
[26] H. Eschrig, *Optimized LCAO Method and the Electronic Structure of Extended Systems* (Akademie, Berlin, 1988).
[27] P. Blaudeck, Th. Frauenheim, G. Jungnickel, and U. Stephan, Solid State Commun. **85**, 1829 (1993).
[28] Th. Frauenheim and P. Blaudeck, Appl. Surf. Sci. **60-61**, 611 (1992).
[29] G. Jungnickel, Th. Frauenheim, D. Porezag, P. Blaudeck, U. Stephan, and R. J. Newport, Phys. Rev. B **50**, 6709 (1994).
[30] G. Jungnickel, Th. Köhler, M. Haase, S. Deutschmann, U. Stephan, P. Blaudeck, and Th. Frauenheim, J. Non-Cryst. Solids **183**, 161 (1995).
[31] Th. Frauenheim, G. Jungnickel, Th. Köhler, and U. Stephan, J. Non-Cryst. Solids **182**, 186 (1995).
[32] Th. Köhler, G. Jungnickel, and Th. Frauenheim, Phys. Rev. B **60**, 10 864 (1999).
[33] F. Weich, J. Widany, and Th. Frauenheim, Phys. Rev. Lett. **78**, 3326 (1997).
[34] J. F. Nye, *Physical Properties of Crystals* (Oxford University Press, 1957).
[35] W. F. A. Besling, A. Goossens, B. Meester, and J. Schoonman, J. Appl. Phys. **83**, 544 (1998).
[36] G. Viera, J. L. Andujar, S. N. Sharma, and E. Bertran, Diamond Relat. Mater. **7**, 407 (1998).
[37] M. Tabbal, P. Merel, S. Moisa, M. Chaker, A. Ricard, and M. Moisan, Appl. Phys. Lett. **69**, 1698 (1996).
[38] V. Hietschold and G. Seifert, Phys. Status Solidi B **129**, K163 (1985).
[39] R. A. Street, *Hydrogenated Amorphous Silicon* (Cambridge University, Cambridge, England, 1991).
[40] J. J. Vlassak and W. D. Nix, J. Mater. Res. **7**, 3242 (1992).
[41] J. A. Taylor, J. Vac. Sci. Technol. A **9**, 2464 (1991).
[42] For Goodfellow product information, check the web site, URL: http://www.goodfellow.com/static/E/SI68.HTML
[43] C. W. Ong, X.-A. Zhao, K. F. Chan, Y. M. Ng, P. W. Chan, C. L. Choy, and R. W. M. Kwok, Thin Solid Films **307**, 152 (1997).
[44] H. Uhlig, M. Frieß, J. Dürr, R. Bellissent, H.-P. Lamparter, F. Aldinger, and S. Steeb, Z. Naturforsch., A: Phys. Sci. **51**, 1179 (1996).
[45] L. C. Chen, D. M. Bhusari, C. Y. Yang, K. H. Chen, T. J. Chuang, M. C. Lin, C. K. Chen, and Y. F. Huang, Thin Solid Films **303**, 66 (1997).
[46] S. Schempp, J. Dürr, P. Lamparter, J. Bill, and F. Aldinger, Z. Naturforsch., A: Phys. Sci. **53**, 127 (1998).